The role of mechanical collapse by cryogenic ball milling on the effect of high-pressure homogenization on the microstructural and texturizing properties of partially pectin-depleted tomato cell wall material

Van Audenhove, J.[a*], Bernaerts, T.[a], Putri, N. I.[a], Van Rooy, L.[a], Van Loey, A. M.[a] and Hendrickx, M. E.[a]**

[a] Laboratory of Food Technology and Leuven Food Science and Nutrition Research Centre (LFoRCe), Department of Microbial and Molecular Systems (M^2S), KU Leuven, Kasteelpark Arenberg 22, Box 2457, 3001, Leuven, Belgium

[*] corresponding author during submission process

jelle.vanaudenhove@kuleuven.be

+32 16 37 32 11

[**] corresponding author after publication

marceg.hendrickx@kuleuven.be

+32 16 32 15 72

Declaration of interest: none

Journal: Food Research International

Abstract

In the current study, the effect of different particle size reduction techniques, namely high-pressure homogenization (HPH) and cryogenic ball milling (CBM), on the microstructural and texturizing properties of the tomato acid-unextractable fraction (AcUF) in suspension was studied. Partial pectin depletion was performed by nitric acid pectin extraction on the alcohol-insoluble residue. In the absence of the aforementioned mechanical treatments, the partially pectin-depleted material, i.e., the AcUF, showed a cellular morphology and a high texturizing potential. By short-time CBM in dry-state, the AcUF was extensively fractured and clumped, resulting in a collapsed structure with negligible texturizing potential and low water binding capacity. In contrast, HPH could disrupt the cell wall network (destroying the cellular morphology) resulting in a continuum of interacting material having very similar texturizing potential and a slightly higher water binding capacity than the AcUF before HPH. Furthermore, the potential of HPH to (re)functionalize the collapsed cryo-ball milled AcUF by its shear-induced disruption was shown. Indeed, the debris-like cell wall remnants could to some extent be reopened by HPH, which resulted in a partial recovery of the original texturizing potential and an improved water binding capacity. However, the potential of HPH at 20 MPa to revert the detrimental effect of CBM decreased with increasing CBM treatment time.

Abbreviations and symbols

AcUF: acid-unextractable fraction

AcUF-CBM0.5: cryogenic ball milled AcUF for 0.5 min

AcUF-CBM1: cryogenic ball milled AcUF for 1 min

AcUF-CBM0.5-HPH: AcUF-CBM0.5 high-pressure homogenized at 20 MPa

AcUF-CBM1-HPH: AcUF-CBM1 high-pressure homogenized at 20 MPa

AcUF-HPH: AcUF high-pressure homogenized at 20 MPa

AIR: alcohol-insoluble residue

Ara: arabinose

CBM: cryogenic ball milling

CWM: cell wall material

DM: degree of methyl esterification

Gal: galactose

Glc: glucose

HPH: high-pressure homogenization

PSD: particle size distribution

Man: mannose

Rha: rhamnose

UA: uronic acid

WBC: water binding capacity

Xyl: xylose

$d_{4,3}$: mean volume-based particle size

G': storage modulus

G": loss modulus

Keywords

Cell wall material

Pectin depletion

High-pressure homogenization

Cryogenic ball milling

Rheology

Water binding capacity

Microscopy

Particle size distribution

1 Introduction

The rheological properties of fruit- and vegetable-based suspensions are highly influenced by the properties of the serum phase and the particle phase. The particle properties can mainly be described in terms of their size (distribution), morphology and deformability (Moelants et al., 2014). The particle size can be reduced by different mechanical treatments, such as high-pressure homogenization (HPH) and ball milling (Gao et al., 2020).

During HPH, a dispersion is forced through a narrow valve under high pressure, which results in particle size reduction because of the high shear forces, cavitation, turbulent flow and velocity gradients (Gao et al., 2020; Levy et al., 2020). This process is mainly applied in the food industry on emulsions to increase the stability and on suspensions to reduce the size of the constituting particles (Levy et al., 2020; Salehi, 2020). Ball milling, in contrast, reduces the particle size due to the impact, grinding force and friction exerted on the material by the moving balls and it is mainly applied in the generation of superfine powders (Gao et al., 2020). This reduction in particle size was observed for

fiber rich particles of different plant sources, such as sugar beet (Huang, Dou, et al., 2018; Huang, Li, et al., 2018), carrot (Chau et al., 2007), asparagus (Chitrakar et al., 2020) and persimmon (Ramachandraiah & Chin, 2016). When milling is performed under cryogenic conditions rather than under ambient conditions, the material becomes more brittle allowing a (faster) formation of finer particles (Balasubramanian et al., 2012).

Different effects of these mechanical techniques on the hydration properties of the impacted particles from fruit and vegetable origin in suspension have been reported. Van Buggenhout et al. (2015) suggested that after HPH an improved interaction with water could occur because of the larger surface of the fragmented particles. Nevertheless, the effect on the water holding or binding capacity seems dependent on the botanical origin, since the impact of HPH on the microstructure and the resulting potential to swell differs among different fruits and vegetables (Bengtsson & Tornberg, 2011; Lopez-Sanchez et al., 2011; Van Audenhove, Bernaerts, Putri, et al., 2021). Regarding the effect of ball milling, Hussain et al. (2018) observed that the water holding capacity of lotus node powder increased with longer milling time, which was also related to the larger surface leading to an increased availability of water binding sites. In contrast, lower water holding/binding capacities were observed after milling by Auffret et al. (1994) for sugar beet fiber, by Chitrakar et al. (2020) for asparagus leaf by-products and by Ramachandraiah & Chin (2016) for persimmon by-products. This could be attributed to the collapse of the porous material during milling, however, also this effect seemed to be dependent on the matrix studied (Auffret et al., 1994).

The relation between the rheological properties of fruit- and vegetable-based suspensions and the size (distribution) of the particles is also not straightforward. On the one hand, Bengtsson & Tornberg (2011) showed for an array of fruits and vegetables that particles with larger surface area obtained by (different numbers of) HPH treatments at 9 MPa was related to a higher storage modulus (G') of the suspension. This could be rationalized as smaller particles have a larger surface area, which allows more interactions than larger particles (Moelants et al., 2014). On the other hand, in the case of apple

and carrot, a decrease in the size and irregularity of the particles (e.g., from cell clusters to single cells to cell fragments) resulted in a less rigid network as shown by the decrease in the viscosity and/or G' of suspensions thereof (Appelqvist et al., 2015; Day et al., 2010; Leverrier et al., 2016). In this context, as stipulated by Moelants et al. (2013), it is important to recognize that in addition to the particle size also other particle properties (e.g., shape, deformability and surface) could influence the network formed in suspension and thus the resulting G'.

The current study compares the effect of two different particle size reduction techniques, namely HPH at low pressure level (20 MPa) and cryogenic ball milling (CBM) with short treatment time, on the microstructural properties and the texturizing potential of partially pectin-depleted tomato cell wall material (CWM). More specifically, the acid-unextractable fraction (AcUF) obtained after acid pectin extraction on the alcohol-insoluble residue (AIR) is studied. In this context, it is shown by Atencio et al. (2021) and Willemsen et al. (2017) for pumpkin pomace and lemon peel, respectively, that the CWM had an improved network forming potential in suspension after partial pectin depletion and that this potential could be further improved by HPH. Tomato was chosen for this work as the stiffness of the network in tomato-based suspensions was generally improved by HPH at relatively low pressure levels (up to around 50-70 MPa) (Augusto et al., 2013; Bayod & Tornberg, 2011; Lopez-Sanchez et al., 2011). To the best of our knowledge, no research has already been performed on the role of CBM on the texturizing potential of (partially pectin-depleted) CWM from fruit or vegetable origin. Auffret et al. (1994) discussed that grinding a fruit or vegetable matrix could result in a collapse of the structure. In the current study, first, the impact of CBM on the microstructure of the tomato AcUF was evaluated and compared with the impact of HPH. Since HPH on a suspension and CBM on a dry material induce different types of disruption (Gao et al., 2020), namely mainly shear and brittle fracture, respectively, it can be expected that the fragmented CWM differs not only in size but also in other microstructural properties, reflecting the different principle of disruption. These different microstructures could have repercussions on the resulting water binding capacity (WBC) and the network forming potential. Secondly, the potential of HPH to (re)functionalize the AcUF impacted by CBM was evaluated by

considering to which extent HPH on suspensions of the cryogenic ball milled material could revert the (detrimental) impact of CBM on the functionality of the AcUF.

2 Material and methods

2.1 Materials

The "San Marzano" tomatoes (*Solanum lycopersicum*) were bought in a local shop. The tomatoes were stored at room temperature for maximally five days before being blanched.

H_2SO_4 (concentration ≥ 95% w/w), disodium tetraborate decahydrate, HCl (0.1 M) and NaOH (0.1 M) were bought from Fisher Scientific (Merelbeke, Belgium). Technical ethanol (99%), technical acetone, Na_2CO_3 and NaOH pellets were obtained from VWR (Leuven, Belgium). 3-phenylphenol and HNO_3 were obtained from Acros Organics (Geel, Belgium), H_2SO_4 (72% w/w) from Alfa Aesar (Kandel, Germany) and NaOH (50% w/w) from J.T. Baker (Gliwice, Poland). Galacturonic acid monohydrate and fucose were bought from Sigma-Aldrich (Diegem, Belgium), rhamnose monohydrate from Acros Organics (Geel, Belgium), arabinose from Fluka Biochemika (Buchs, Switzerland), galactose from Merck (Darmstadt, Germany), glucose monohydrate from Riedel-de-Haën (Seelze, Germany), xylose from UCB (Leuven, Belgium) and mannose from Fluka Analytical (Buchs, Switzerland). A Simplicity™ 150 system provided the ultrapure water (organic free, 18.2 MΩ·cm resistance). All chemicals used were of analytical grade, except when it is mentioned otherwise.

2.2 Blanching of the tomato tissue

The tomato was high-temperature blanched (Christiaens et al., 2012). For this, the washed tomatoes were cut in slices with a thickness of 5 mm and vacuum packed in a plastic bag. Next, the slices were blanched for 8 min at 95°C, cooled in an ice bath, frozen with liquid nitrogen and stored at -40 °C until further use.

2.3 Generation of the alcohol-insoluble residue and the acid-unextractable fraction

The AIR was prepared based on the method described by McFeeters & Armstrong (1984). Before the AIR preparation, the slices were thawed, mixed in a laboratory blender two times for three seconds (Waring Commercial, Torrington, CT, USA) and filtered over a 1 mm sieve to remove the peels and seeds. To 60 g of the tomato tissue, 192 mL of technical ethanol was added and mixed three times for 6 s (Mixer B-400, Büchi, Flawil, Germany). After vacuum filtration (MN615 filter paper, Macherey-Nagel, Düren, Germany), two precipitates were re-dispersed together in 192 mL of technical ethanol. After mixing (three times for 6 s) and vacuum filtration, the obtained precipitate was dispersed in technical acetone for 10 min under continuous stirring. The precipitate was recovered by vacuum filtration and dried overnight at 40 °C. The AIR, grounded with mortar and pestle, was stored until further use.

The AcUF was obtained as the unextractable fraction after acid pectin extraction on the AIR. The extraction conditions were the same as applied by Willemsen et al. (2017). Briefly, 60 g of the AIR was brought into 4 L of deionized water (80 °C) and stirred for 30 min. Next, the pH was adjusted to 1.6 with 7 M HNO_3 and the extraction at 80 °C was continued for 1 h under continuous stirring. The separation of the supernatant and pellet and the washing of the pellet were performed as described by Van Audenhove, Bernaerts, De Smet, et al. (2021). In short, the extraction mixture was cooled in an ice bath to room temperature and subsequently centrifuged at 8000g for 10 min (Avanti JXN-26, Beckman Coulter Inc, Indianapolis, IN, USA). Next, 3 L of deionized water was added to the pellet. After being stirred for 10 min, the mixture was centrifuged again (8000g for 10 min). The AcUF was vacuum-packed, frozen with liquid nitrogen and stored at -40 °C until being lyophilized (Alpha 2-4 LSC plus, Christ, Osterode am Harz, Germany). The lyophilized AcUF was stored in a desiccator until further use.

2.4 Chemical characterization

2.4.1 Analysis of the uronic acid content of the acid-unextractable fraction

The hydrolysis of the lyophilized AcUF was based on the method by Ahmed & Labavitch (1977). Overnight, 10 mg of the AcUF was hydrated in 2 mL of deionized water. To initiate the hydrolysis, 8 mL of sulfuric acid (95%) was added to the sample in an ice bath under continuous stirring. After 5 min, another 2 mL of deionized water was added to the sample. The hydrolysis was stopped after 1 h by diluting the hydrolysate to 100 mL with deionized water. The uronic acid (UA) content of the diluted hydrolysate was determined based on the method described by Blumenkrantz & Asboe-Hansen (1973). To 0.6 mL of the diluted hydrolysate, 3.6 mL of sulphuric acid (95%) with sodium tetraborate (0.0125 M) was added. The mixture was heated for 5 min at 100 °C. After being cooled in an ice bath, 60 µL of m-hydroxydiphenyl (0.15% w/v) in 0.5% w/v NaOH (or only 0.5% w/v NaOH in the case of the blank) was added. The mixture was then vortexed for 1 min and, after 1 min waiting, its absorbance was obtained at 520 nm (Spectrophotometer Genesys 30 Vis, Thermo Fisher, Waltham, MA, USA). External standards of galacturonic acid were used to calculate the UA content.

2.4.2 Analysis of the monosaccharide composition of the acid-unextractable fraction

Saeman hydrolysis was performed on 3 mg of lyophilized AcUF to hydrolyze all polysaccharides present in the AcUF. The hydrolysis procedure consisted of an incubation step for 1 h at 30 °C in 150 µL of 72% w/w sulfuric acid followed by hydrolysis at 121 °C in 4% (w/v) sulfuric acid for 1 h (Yeats et al., 2016). The content of rhamnose (Rha), arabinose (Ara), galactose (Gal), glucose (Glc), xylose (Xyl) and mannose (Man) was determined using high performance anion exchange chromatography (ICS-6000, Dionex, Sunnyvale, CA, USA) with pulsed amperometric detection (ED50 electrochemical detector, Dionex, Sunnyvale, CA, USA). The hydrolysis and the chromatographic analysis were performed exactly as described by Van Audenhove, Bernaerts, Putri, et al. (2021).

2.4.3 Degree of methyl esterification of the acid-unextractable fraction

The method of Kyomugasho et al. (2015) was used to determine the degree of methyl esterification (DM) of the residual pectin by Fourier transform infrared spectroscopy (FT-IR spectrophotometer, IRAffinity-1, Shimadzu, Tokyo, Japan). The preparative steps were performed exactly as described by Van Audenhove, Bernaerts, Putri, et al., (2021). The calibration curve between the DM and the absorption intensity at 1600 cm^{-1} and 1740 cm^{-1} (after deconvolution) developed by Kyomugasho et al. (2015) was used to calculate the DM of the AcUF.

2.5 Particle size reduction by cryogenic ball milling and high-pressure homogenization

Different (combinations of) particle size reduction techniques were performed on the AcUF. An overview of the treatments applied is schematically shown in **Figure 1**, wherein the naming of the samples is also included. As a control, untreated lyophilized AcUF was analyzed and denoted as the AcUF. The other part was, in the dry state, treated either by CBM for 0.5 or 1 min, referred to as the AcUF-CBM0.5 and AcUF-CBM1 respectively, or by HPH (in a dispersed state) at 20 MPa referred to as the AcUF-HPH. Furthermore, part of the AcUF-CBM0.5 and AcUF-CBM1 was high-pressure homogenized at 20 MPa, denoted as the AcUF-CBM0.5-HPH and AcUF-CBM1-HPH respectively.

2.5.1 Cryogenic ball milling of the lyophilized acid-unextractable fraction

For each run in the cryogenic ball mill (CryoMill, Retsch GmbH, Haan, Germany), 1 g of the lyophilized AcUF was transferred in a hardened steel jar together with three hardened steel balls (diameter: 15 mm). The AcUF was cooled by liquid nitrogen flowing over the grinding jar enclosed by a cooling jacket. After precooling of the sample at frequency 5 Hz controlled by an in-build sensor in the device, the AcUF was cryogenically ball milled for 0.5 min at 30 Hz or 1 min at 30 Hz under steady supply of liquid nitrogen.

2.5.2 Preparation and high-pressure homogenization of the suspensions of (cryogenic ball milled) lyophilized acid-unextractable fraction

Deionized water was added to the AcUF, AcUF-CBM0.5 or AcUF-CBM1 to obtain 2% (w/w) concentration. The pH of the suspensions, which was originally around 2.3, was adjusted to 4.5 using 2 M Na_2CO_3. The suspension prepared with the AcUF was stored overnight at room temperature and mixed for 10 min at 8000 rpm (Ultra Turrax T25, IKA, Staufen, Germany). The suspensions prepared with the AcUF-CBM0.5 and AcUF-CBM1 were continuously stirred overnight. Thereafter, part of the suspensions prepared from the AcUF, AcUF-CBM0.5 and AcUF-CBM1 were high-pressure homogenized (Panda 2k, GEA Niro Soavi, Parma, Italy) at 20 MPa (Van Audenhove, Bernaerts, Putri, et al., 2021).

2.6 Characterization of the microstructural and functional properties

The characterization of the microstructural and functional properties of the suspensions of the differently treated AcUFs was performed exactly as described in Van Audenhove, Bernaerts, Putri, et al. (2021). In the following sections, the methods are described briefly.

2.6.1 Microscopic visualization

To improve the clarity of the visualization of the microstructural attributes of the particles in suspension, the suspension was diluted to 0.6% (w/w) using deionized water at pH 4.5 (adjusted with 0.1 M HCl) and stirred for at least 1 h. Next, 100 µL of this diluted suspension was pipetted on a microscope slide and at least ten pictures were taken at magnification 10x in differential interference contrast microscopy mode (Olympus BX-51, Olympus Optical Co. Ltd., Tokyo, Japan) using a XC-50 digital camera.

2.6.2 Particle size distribution analysis

Laser diffraction (Laser Diffraction Particle Size Analyzer, LS 13 320, Beckman Coulter Inc., Indianapolis, IN, USA) was used to determine the volume-based particle size distribution (PSD) and the average volume-based particle size ($d_{4,3}$). Some droplets of the suspension were added to a tank filled with

deionized water until an obscuration of around 8-10% was reached. Two runs taking 90 s each at pump speed 30% were performed in sequence. The PSD (ranging from 0.04 to 2000 µm) was calculated using the Fraunhofer model based on the diffraction of the laser light. However, to exclude weak aggregation that would affect the PSD obtained, only the data from the second run was retained. The particle size analysis was performed in duplicate.

2.6.3 Rheological analysis

In short, the rheological analysis (MCR 302, Anton Paar, Graz, Austria) consisted of a sequence of steps and made use of the rough concentric cylindric geometry designed by Willemsen et al. (2018). When the suspension was loaded, a pre-shear (10 s^{-1}) was applied for 1 min. After 1 min waiting time, this was followed by 3 min in the oscillatory regime at constant angular frequency 10 rad/s and strain 0.1%. Next, a frequency sweep was performed with logarithmically decreasing (7 points per decade) angular frequency from 100 to 0.1 rad/s at constant strain 0.1%. Then, the suspension was kept in the oscillatory regime for 1 min at constant angular frequency 10 rad/s and strain 0.1%. Finally, a strain sweep was performed with logarithmically increasing (7 points per decade) strain from 0.01 to 100% and at constant angular frequency 10 rad/s. The data of the strain sweep were used to validate that the frequency sweep was performed within the linear viscoelastic region and to calculate the critical strain by interpolation, which is defined as the strain at which the G' decreased to 90% of the plateau value at low strain (Van Audenhove, Bernaerts, Putri, et al., 2021). The rheological analysis was performed in duplicate.

2.6.4 Measurement of water binding capacity

The WBC was determined by centrifugation at 1000g for 30 min at 25 °C (LUMiFuge, LUM GmbH, Berlin, Germany) on the 2% (w/w) suspension. The suspension was brought in a polycarbonate cuvette. After centrifugation, the WBC was calculated based on the mass of the added suspension and the mass of supernatant obtained after centrifugation using eq. 1. The measurement of the WBC was performed in duplicate.

$$WBC = \frac{mass\ suspension \cdot 0.98 - mass\ of\ supernatant}{mass\ suspension \cdot 0.02}$$ [eq. 1]

in which WBC is the water binding capacity [g water/g].

2.7 Statistical analysis

Each sample was at least measured twice, leading to the reported average and standard deviation. The Tukey's range test was used to evaluate the reported significances of the differences between means with 95% confidence interval ($p < 0.05$) (JMP Pro 15, SAS Institute Inc., Cary, NC, USA).

3 Results and discussion

3.1 Chemical properties

The monosaccharide composition and the DM of the AcUF is shown in **Table 1**. The composition is very similar to what has previously been reported for tomato AcUF by Van Audenhove, Bernaerts, De Smet, et al. (2021). The most abundant monosaccharide was Glc which can be attributed to the high cellulose and hemicellulose content in the AcUF. Although this fraction was partially depleted in pectin, still a relevant amount of pectin (as evaluated by the UA content) was retained in this fraction. The residual pectin had a DM of 55.6 ± 2.8%.

3.2 Effect of cryogenic ball milling and high-pressure homogenization on the microstructure of the acid-unextractable fraction in suspension

The micrographs of the suspensions (at 0.6% w/w) of the differently treated AcUFs are shown in **Figure 2**. The microstructure of the AcUF was mainly characterized by intact particles still showing a cell-like morphology, as was also observed for the AcUF of other fruits and vegetables before HPH (Van Audenhove, Bernaerts, Putri, et al., 2021). The intactness of the cell wall shape thus seemed to be hardly affected by the acid pectin depletion. The $d_{4,3}$ of the particles in the AcUF was 384 ± 2 µm (**Figure 3**). This value is in accordance with the average cell size of San Marzano tomato estimated as

400 x 600 µm by Becker, Miers, Nutting, Dietrich, & Wagner (1972) and the $d_{4,3}$ of approximately 400 µm for tomato single cells in dispersion reported by Lopez-Sanchez, Chapara, Schumm, & Farr (2012).

The micrographs (**Figure 2**) of the AcUF-CBM0.5 and AcUF-CBM1 clearly showed small cell wall fragments, resulting from the pulverizing action of the CBM treatment on the partially pectin-depleted cell walls (Jiang et al., 2020; Wang et al., 2020). These fragments could be described as "debris" occurring separately and not showing a substantial tendency to aggregate. Furthermore, the size of the fragments was, as expected, clearly smaller after 1 min compared to the size after 0.5 min treatment time. This was reflected by the shift of the PSD to smaller particle sizes with increasing milling time (**Figure 4**) and by the decrease in $d_{4,3}$ to 147 ± 8 and 65 ± 3 µm after CBM for 0.5 and 1 min, respectively. A decrease in the particle size of plant material with increasing milling time was also reported by other authors (Chau et al., 2007; Hussain et al., 2018; Jiang et al., 2020; Wang et al., 2020), except for a very long treatment time for which agglomeration was reported due to the high surface energy of the very small particles (Chitrakar et al., 2020; Liu et al., 2019). The fast decrease in the particle size (62% and 83% after CBM for 0.5 and 1 min respectively, based on the $d_{4,3}$) during the milling process could be attributed to the cryogenic conditions leading to the higher brittleness of the material as it is milled at a temperature lower than its glass transition temperature (Balasubramanian et al., 2012; Ghodki & Goswami, 2016; Singh et al., 2018). By Ghodki & Goswami (2016), it was shown for black pepper that with decreasing processing temperature (range from 40 °C to -120 °C), smaller particles were obtained and less energy was needed for the grinding process.

After mechanical treatment of the AcUF by HPH at 20 MPa, the cellular morphology was lost (**Figure 2**, AcUF-HPH). Interestingly, while part of the AcUF was clearly disrupted resulting in a continuum of CWM, fiber-like cell wall structures could still be discerned after HPH at 20 MPa indicating that part of the cell walls was only broken and deformed but still retained its integrity to some extent. This wide variation in the microstructural attributes obtained after HPH at 20 MPa was reflected in the PSD of the AcUF-HPH which had not only a peak at around 100 µm but also a prominent shoulder at the

dimensions of cell-like particles in the AcUF (at around 400 µm) (**Figure 4**). When comparing the microstructure of the AcUF-HPH, AcUF-CBM0.5 and AcUF-CBM1, it is clear that the impact of the treatments applied on the AcUF were completely different. While the microstructural attributes of the AcUF after disruption by HPH allowed the formation of a continuum of interacting and entangled CWM, this seemed not to apply in the case of the collapsed debris-like particles obtained after CBM.

When comparing the micrographs of the AcUF-CBM0.5-HPH and AcUF-CBM1-HPH suspensions with the respective non-homogenized AcUF-CBM0.5 and AcUF-CBM1 suspensions, it is clear that the AcUF-CBM (at both treatment times) could be further disintegrated by HPH, which is confirmed by a shift to smaller particle size (**Figure 4**). Related to the smaller size of the cryo-ball milled AcUF after longer milling time, the $d_{4,3}$ of the AcUF-CBM1-HPH was smaller (29 ± 0.1 µm) than for the AcUF-CBM0.5-HPH (57 ± 1 µm). More specifically, after HPH, instead of remnants with defined edges (as observed after CBM), structures with very irregular shapes were observed (**Figure 2**). This can again be related to the different impact of CBM and HPH on the microstructure of the AcUF. Indeed, instead of further fracturing and/or compacting of the cell wall remnants (as observable between the AcUF-CBM0.5 and AcUF-CBM1), the fragments were teared apart by the shear forces into multiple smaller fragments with a more open structure (not having these well-defined edges). As a consequence, it can be expected that the collapse of the AcUF microstructure induced by CBM is (partially) reverted by HPH.

3.3 Effect of cryogenic ball milling and high-pressure homogenization on the functional properties of the acid-unextractable fraction in suspension

3.3.1 Water binding capacity

The WBC of the AcUF was 40 ± 2 g water/g. By CBM, the WBC was decreased to 19 ± 1 g water/g for the AcUF-CBM0.5 and to 15 ± 0.05 g water/g for the AcUF-CBM1 (**Figure 5**). This detrimental effect of CBM on the WBC of the AcUF could be understood as follows. First, as a consequence of the loss of the integrity of the partially pectin-depleted cell walls by CBM, the amount of water being originally entrapped by the cellular structures in the AcUF (Van Audenhove, Bernaerts, Putri, et al., 2021) is

expected to be released in case of the AcUF-CBM0.5 and AcUF-CBM1. Second, water can interact with fibrous material by hydrogen and ionic bonds, by hydrophobic interactions and can be bound in capillaries (Chaplin, 2003; Thebaudin et al., 1997). *In planta*, the cell wall polymers form a porous network (Carpita et al., 1979). Moreover, given the considerable removal of pectin from the cell wall network, a high amount of pores and voids could be expected in the AcUF (Willemsen et al., 2017). However, due to the collision impact during CBM, the physical structure of the cell wall network in the AcUF was most probably not only fractured but also collapsed, as was also suggested by Auffret et al. (1994) for sugar beet fiber. This collapse of the porous network of the partially pectin-depleted cell walls and the clumping of the material induced by CBM probably resulted in a lower surface area accessible to water and, as a consequence, to a decrease in the WBC. This loss of the porous structure with longer milling time was also described by Jiang et al. (2020) for onion peel powder.

In contrast to CBM, HPH resulted in a small increase in the WBC (**Figure 5**). A higher abundance of water binding sites on the AcUF after HPH, and thus an improved WBC, could be expected since the impact of HPH resulted in a more accessible cell wall structure and a decrease in the particle size (Van Buggenhout et al., 2015). However, the increase in the WBC was limited, as the original entrapment of water by the cellular structure was impaired due to the reduced cell wall integrity after HPH (Van Audenhove, Bernaerts, Putri, et al., 2021).

Furthermore, HPH was also performed on the suspended cryo-ball milled AcUF. The observation that the WBC of the AcUF-CBM0.5-HPH and AcUF-CBM1-HPH was clearly higher than for the AcUF-CBM0.5 and AcUF-CBM1 (**Figure 5**) shows again the different impact of the two treatments on the AcUF. However, the WBC could not be restored to the same level as for the homogenized AcUF without preceding CBM, indicating that HPH at 20 MPa could only partially unlock the collapsed structure created by CBM. Interestingly, although the particle size was lower, the WBC was lower for the AcUF-CBM1-HPH than for the AcUF-CBM0.5-HPH. This observation highlights that the ability to facilitate the

interaction between CWM and water by re-opening of the collapsed structure by HPH at 20 MPa decreased with increasing preceding CBM treatment time.

3.3.2 Viscoelastic properties

The dependency of the viscoelastic moduli on the angular frequency is shown in **Figure 6**. For the AcUF suspension, a low dependency of the G' on the angular frequency was observed, which was also observed for suspensions prepared from AcUF of other matrices (Van Audenhove, Bernaerts, Putri, et al., 2021) and other suspensions of fruit and vegetable CWM (Kotcharian et al., 2004; Kunzek et al., 1999; Pickardt et al., 2004; Redgwell et al., 2008; Vetter & Kunzek, 2003; Wang et al., 2018). The G' was clearly higher than the loss modulus (G") for the AcUF suspension and the high-pressure homogenized suspensions (the loss factor was in the range of 0.14 to 0.20 at 10 rad/s), which indicates the gel-like character of the suspensions. Different behavior was observed for the AcUF-CBM0.5 and AcUF-CBM1 suspensions. Indeed, not only the loss factor of the AcUF-CBM0.5 was much higher (namely, 0.37 ± 0.05), but also a cross-over point was observed between G' and G" at higher frequency. The negligible G' implicates that the cryo-ball milled particles in suspension did not have the potential to form a network with a significant stiffness. While sedimentation of the particles was limited in the AcUF-CBM0.5 suspension, substantial sedimentation occurred within the rheological measurement time frame (around 30 min) in the AcUF-CBM1 suspension. Due to the poor stability of this suspension, no data on the viscoelastic properties of the AcUF-CBM1 suspension was presented. Furthermore, for the AcUF-CBM0.5 suspension, data obtained at frequencies higher than 60 rad/s were not meaningful and are therefore excluded from **Figure 6**. The frequency sweeps were performed within the linear viscoelastic region, since the critical strain was well above 0.1% for all the suspensions (**Figure 7**). As the trend of all the curves in **Figure 6** was very similar except for the behavior of the AcUF-CBM0.5 and AcUF-CBM1 suspension, the texturizing potential of the AcUF after the different mechanical treatments was evaluated by comparing the G' at 10 rad/s.

The G' of the suspensions (at angular frequency 10 rad/s and strain 0.1%) prepared with the AcUF after different mechanical treatments is shown in **Figure 8**. The G' of the AcUF suspension was 1726 ± 127 Pa. A tremendous decrease in the G' of the suspension was observed when the AcUF was subjected to CBM. While the large pectin-depleted cell-like particles present in the AcUF could form a network by close packing (Appelqvist et al., 2015; Lopez-Sanchez et al., 2012), which resulted in a high G', the small particles in the AcUF-CBM0.5 and AcUF-CBM1 did not have the ability to form a particle network in suspension. A prominent effect of the particle size on the G' of these systems has also been shown in our previous study on the texturizing potential of AcUFs originating from different botanical origins, in which it was observed that the G' of suspensions prepared from AcUF with larger cell-like particles (e.g., for apple and onion) was much higher than for smaller cell-like particles (e.g., for pumpkin) (Van Audenhove, Bernaerts, Putri, et al., 2021).

Notwithstanding the clear effect of HPH on the AcUF microstructure (**Figure 2**), the G' of the suspension was almost unaffected by HPH. In other words, the disruption of the cell-like AcUF structure, thus facilitating other (physical) interactions (Augusto et al., 2012, 2013; Tan & Kerr, 2015), did not result in a higher texturizing potential of the material. Nevertheless, the different nature of the network was reflected by the prominent increase in the critical strain upon HPH (**Figure 7**). By Lopez-Sanchez & Farr (2012), it was also shown for tomato that a suspension of cell fragments prepared by HPH had a higher critical strain than a suspension of individual cells, which was attributed to the ability of these ribbon-like cell wall fragments to form entanglements and to the increase in the surface available for particle-particle interactions.

Although the PSDs of the AcUF-HPH and AcUF-CBM0.5 were quite similar (**Figure 4**), the difference between the G' of the respective suspensions covered orders of magnitude. This observation is a very clear manifestation of the role of the particle size reduction technique applied to the tomato AcUF on the resulting functional properties. This is a consequence of the greatly differing impact on the microstructure while reaching a certain size reduction (**Figure 2**). Indeed, whereas the shear-induced

disruption of the cell wall structure by HPH could facilitate the formation of cell wall particle interactions, CBM resulted in a mechanical collapse of the initial structure (**Figure 2**). This collapse originated from the fracturing and clumping effect induced by CBM on the original cell wall, which probably has a twofold effect on the potential of the AcUF to form a volume-spanning network. On the one hand, in contrast to HPH, CBM probably resulted in the inability of the material to form entanglements, which is supported by the observation that the critical strain of the AcUF-CBM0.5 suspension was clearly lower than for the AcUF-HPH suspension and similar to what was obtained for the AcUF, in which the pectin-depleted cell walls were still highly intact. On the other hand, in line with the observed decrease in the WBC (**Figure 5**), a decrease in the surface area available for particle-particle interactions can be expected.

A substantial increase in the texturizing potential of the AcUF-CBM0.5 and AcUF-CBM1 by HPH was observed, which indicates that HPH has the potential to partially (re)functionalize the collapsed structure, along with a further particle size reduction. However, when compared to the G' of the AcUF-HPH suspension, it is clear that the extent of the recovery of the texturizing potential was limited and much lower than what was observed in case of the WBC. Furthermore, the extent of fracturing during CBM also affected the G' of the resulting suspension after HPH, as the AcUF-CBM0.5-HPH suspension had a higher G' than the AcUF-CBM1-HPH suspension. Although HPH had the potential to unlock the partially pectin-depleted CWM to a certain extent, both from the original pectin-depleted cell wall network as well as from the fractured and collapsed cell wall remnants, these observations also stipulate the great role of the particle size in the texturizing potential of the disrupted AcUF. Indeed, a continuum of aggregating CWM can be observed for each high-pressure homogenized suspension, however, it can be expected that particles with smaller dimensions (as is the case for the AcUF-CBM0.5-HPH and AcUF-CBM1-HPH) have less interaction zones and can therefore possibly interact with fewer particles. In spite of its lower G', the AcUF-CBM1-HPH suspension had the highest critical strain thus indicating that the network formed by the smallest particles obtained after HPH in the current study seemed to have the highest resistance against deformation.

4 Conclusions

The effect of CBM and HPH on the microstructural and functional properties of the AcUF of tomato was investigated in the current study. In absence of these mechanical treatments, the particles of this partially pectin-depleted CWM still displayed cell-like morphology. Both treatments had a significant yet very different effect on the microstructure. By CBM, the lyophilized AcUF was clearly fractured into small particles with clearly defined edges. In contrast, by HPH, the original network structure was opened resulting in a continuum of the disrupted AcUF together with the presence of fiber-like structures. Furthermore, the results showed that the differences in the microstructural attributes after the different particle size reduction techniques, due to the distinct nature of the respective impact (mainly brittle fracture versus mainly shear), had a very prominent repercussion on the functional properties in suspension, namely the WBC and the creation of a stiff network in suspension. The substantial decrease in the WBC and the negligible G' together with the very dense and debris-like appearance of the fragments, indicated that CBM resulted in a mechanical collapse of the cell wall network. Although HPH of a suspension of the non-treated lyophilized AcUF only slightly improved the functional properties, the collapsed AcUF structures obtained after CBM could partially be unlocked by subsequent HPH. This resulted in a prominent increase in the G', although the resulting G' was still relatively low, the critical strain and the WBC. In line with the higher extent of fracturing by CBM after longer treatment time (1 min versus 0.5 min), the potential of HPH at 20 MPa to (re)functionalize the material was lower after longer preceding CBM. For further research, it could be interesting to evaluate whether CBM and the combination of CBM and HPH have similar effects on the texturizing potential of the (partially pectin-depleted) CWM of other matrices to what was observed for tomato. Furthermore, studies evaluating other functionalities, like emulsion stabilizing properties for example, of these cell wall material structures could be very relevant to gain more insight into possible applications of these mechanical treatments in the food industry.

Acknowledgements

J. Van Audenhove is funded by the Research Foundation Flanders (FWO), grant number 1134619N. T. Bernaerts is funded by the Research Foundation Flanders (FWO), grant number 1252221N. The funding source had no role in the study design, collection, analysis and interpretation of the data, the writing of this manuscript or in the decision to submit the manuscript for publication.

References

Ahmed, A. E. R., & Labavitch, J. M. (1977). A simplified method for accurate determination of cell wall uronide content. *Journal of Food Biochemistry*, *1*(4), 361–365. https://doi.org/10.1111/j.1745-4514.1978.tb00193.x

Appelqvist, I. A. M., Cochet-Broch, M., Poelman, A. A. M., & Day, L. (2015). Morphologies, volume fraction and viscosity of cell wall particle dispersions particle related to sensory perception. *Food Hydrocolloids*, *44*, 198–207. https://doi.org/10.1016/j.foodhyd.2014.09.012

Atencio, S., Bernaerts, T., Liu, D., Reineke, K., Hendrickx, M., & Van Loey, A. (2021). Impact of processing on the functionalization of pumpkin pomace as a food texturizing ingredient. *Innovative Food Science & Emerging Technologies*, *69*, 102669. https://doi.org/10.1016/j.ifset.2021.102669

Auffret, A., Ralet, M.-C., Guillon, F., Barry, J.-L., & Thibault, J.-F. (1994). Effect of Grinding and Experimental Conditions on the Measurement of Hydration Properties of Dietary Fibres. *LWT - Food Science and Technology*, *27*(2), 166–172. https://doi.org/10.1006/fstl.1994.1033

Augusto, P. E. D., Ibarz, A., & Cristianini, M. (2012). Effect of high pressure homogenization (HPH) on the rheological properties of tomato juice: Time-dependent and steady-state shear. *Journal of Food Engineering*, *111*(4), 570–579. https://doi.org/10.1016/j.jfoodeng.2012.03.015

Augusto, P. E. D., Ibarz, A., & Cristianini, M. (2013). Effect of high pressure homogenization (HPH) on the rheological properties of tomato juice: Viscoelastic properties and the Cox-Merz rule. *Journal of Food Engineering*, *114*(1), 57–63. https://doi.org/10.1016/j.jfoodeng.2012.07.025

Balasubramanian, S., Gupta, M. K., & Singh, K. K. (2012). Cryogenics and its Application with Reference to Spice Grinding: A Review. *Critical Reviews in Food Science and Nutrition*, *52*(9), 781–794. https://doi.org/10.1080/10408398.2010.509552

Bayod, E., & Tornberg, E. (2011). Microstructure of highly concentrated tomato suspensions on homogenisation and subsequent shearing. *Food Research International*, *44*(3), 755–764. https://doi.org/10.1016/j.foodres.2011.01.005

Becker, R., Miers, J. C., Nutting, M.-D., Dietrich, W. C., & Wagner, J. R. (1972). Consistency of tomato products. 7. Effects of acidification on cell walls and cell breakage. *Journal of Food Science*, *37*(1), 118–125. https://doi.org/10.1111/j.1365-2621.1972.tb03399.x

Bengtsson, H., & Tornberg, E. (2011). Physicochemical characterization of fruit and vegetable fiber suspensions. I: effect of homogenization. *Journal of Texture Studies*, *42*(4), 268–280. https://doi.org/10.1111/j.1745-4603.2010.00275.x

Blumenkrantz, N., & Asboe-Hansen, G. (1973). New method of quantitative determination of uronic acids. *Analytical Biochemistry*, *54*(2), 484–489. https://doi.org/10.1016/0003-2697(73)90377-1

Carpita, N., Sabularse, D., Montezinos, D., & Delmer, D. P. (1979). Determination of the Pore Size of Cell Walls of Living Plant Cells. *Science*, *205*(4411), 1144–1147. https://doi.org/10.1126/science.205.4411.1144

Chaplin, M. F. (2003). Fibre and water binding. *Proceedings of the Nutrition Society*, *62*(1), 223–227. https://doi.org/10.1079/PNS2002203

Chau, C.-F., Wang, Y.-T., & Wen, Y.-L. (2007). Different micronization methods significantly improve the functionality of carrot insoluble fibre. *Food Chemistry*, *100*(4), 1402–1408. https://doi.org/10.1016/j.foodchem.2005.11.034

Chitrakar, B., Zhang, M., Zhang, X., & Devahastin, S. (2020). Bioactive dietary Fiber powder from asparagus leaf by-product: Effect of low-temperature ball milling on physico-chemical, functional

and microstructural characteristics. *Powder Technology*, *366*, 275–282. https://doi.org/10.1016/j.powtec.2020.02.068

Christiaens, S., Van Buggenhout, S., Houben, K., Chaula, D., Van Loey, A. M., & Hendrickx, M. E. (2012). Unravelling process-induced pectin changes in the tomato cell wall: An integrated approach. *Food Chemistry*, *132*(3), 1534–1543. https://doi.org/10.1016/j.foodchem.2011.11.148

Day, L., Xu, M., Øiseth, S. K., Hemar, Y., & Lundin, L. (2010). Control of morphological and rheological properties of carrot cell wall particle dispersions through processing. *Food and Bioprocess Technology*, *3*(6), 928–934. https://doi.org/10.1007/s11947-010-0346-0

Gao, W., Chen, F., Wang, X., & Meng, Q. (2020). Recent advances in processing food powders by using superfine grinding techniques: A review. *Comprehensive Reviews in Food Science and Food Safety*, *19*(4), 2222–2255. https://doi.org/10.1111/1541-4337.12580

Ghodki, B. M., & Goswami, T. K. (2016). Effect of grinding temperatures on particle and physicochemical characteristics of black pepper powder. *Powder Technology*, *299*, 168–177. https://doi.org/10.1016/j.powtec.2016.05.042

Huang, X., Dou, J., Li, D., & Wang, L. (2018). Effects of superfine grinding on properties of sugar beet pulp powders. *LWT*, *87*, 203–209. https://doi.org/10.1016/j.lwt.2017.08.067

Huang, X., Li, D., & Wang, L. (2018). Effect of particle size of sugar beet pulp on the extraction and property of pectin. *Journal of Food Engineering*, *218*, 44–49. https://doi.org/10.1016/j.jfoodeng.2017.09.001

Hussain, S., Li, J., Jin, W., Yan, S., & Wang, Q. (2018). Effect of micronisation on dietary fibre content and hydration properties of lotus node powder fractions. *International Journal of Food Science & Technology*, *53*(3), 590–598. https://doi.org/10.1111/ijfs.13632

Jiang, G., Ramachandraiah, K., Wu, Z., Li, S., & Eun, J.-B. (2020). Impact of ball-milling time on the physical properties, bioactive compounds, and structural characteristics of onion peel powder.

Food Bioscience, *36*(May), 100630. https://doi.org/10.1016/j.fbio.2020.100630

Kotcharian, A., Kunzek, H., & Dongowski, G. (2004). The influence of variety on the enzymatic degradation of carrots and on functional and physiological properties of the cell wall materials. *Food Chemistry*, *87*(2), 231–245. https://doi.org/10.1016/j.foodchem.2003.11.015

Kunzek, H., Kabbert, R., & Gloyna, D. (1999). Aspects of material science in food processing: changes in plant cell walls of fruits and vegetables. *Zeitschrift Für Lebensmitteluntersuchung Und - Forschung A*, *208*(4), 233–250. https://doi.org/10.1007/s002170050410

Kyomugasho, C., Christiaens, S., Shpigelman, A., Van Loey, A. M., & Hendrickx, M. E. (2015). FT-IR spectroscopy, a reliable method for routine analysis of the degree of methylesterification of pectin in different fruit- and vegetable-based matrices. *Food Chemistry*, *176*, 82–90. https://doi.org/10.1016/j.foodchem.2014.12.033

Leverrier, C., Almeida, G., Espinosa-Muñoz, L., & Cuvelier, G. (2016). Influence of Particle Size and Concentration on Rheological Behaviour of Reconstituted Apple Purees. *Food Biophysics*, *11*(3), 235–247. https://doi.org/10.1007/s11483-016-9434-7

Levy, R., Okun, Z., & Shpigelman, A. (2020). High-Pressure Homogenization: Principles and Applications Beyond Microbial Inactivation. *Food Engineering Reviews*. https://doi.org/10.1007/s12393-020-09239-8

Liu, H., Chen, X., Ji, G., Yu, H., Gao, C., Han, L., & Xiao, W. (2019). Mechanochemical deconstruction of lignocellulosic cell wall polymers with ball-milling. *Bioresource Technology*, *286*(March), 121364. https://doi.org/10.1016/j.biortech.2019.121364

Lopez-Sanchez, P., Chapara, V., Schumm, S., & Farr, R. (2012). Shear Elastic Deformation and Particle Packing in Plant Cell Dispersions. *Food Biophysics*, *7*(1), 1–14. https://doi.org/10.1007/s11483-011-9237-9

Lopez-Sanchez, P., & Farr, R. (2012). Power Laws in the Elasticity and Yielding of Plant Particle

Suspensions. *Food Biophysics*, *7*(1), 15–27. https://doi.org/10.1007/s11483-011-9238-8

Lopez-Sanchez, P., Nijsse, J., Blonk, H. C. G., Bialek, L., Schumm, S., & Langton, M. (2011). Effect of mechanical and thermal treatments on the microstructure and rheological properties of carrot, broccoli and tomato dispersions. *Journal of the Science of Food and Agriculture*, *91*(2), 207–217. https://doi.org/10.1002/jsfa.4168

McFeeters, R. F., & Armstrong, S. A. (1984). Measurement of pectin methylation in plant cell walls. *Analytical Biochemistry*, *139*(1), 212–217. https://doi.org/10.1016/0003-2697(84)90407-X

Moelants, K. R. N., Cardinaels, R., Jolie, R. P., Verrijssen, T. A. J., Van Buggenhout, S., Zumalacarregui, L. M., Van Loey, A. M., Moldenaers, P., & Hendrickx, M. E. (2013). Relation between particle properties and rheological characteristics of carrot-derived suspensions. *Food and Bioprocess Technology*, *6*(5), 1127–1143. https://doi.org/10.1007/s11947-011-0718-0

Moelants, K. R. N., Cardinaels, R., Van Buggenhout, S., Van Loey, A. M., Moldenaers, P., & Hendrickx, M. E. (2014). A Review on the relationships between processing, food structure, and rheological properties of plant-tissue-based food suspensions. *Comprehensive Reviews in Food Science and Food Safety*, *13*(3), 241–260. https://doi.org/10.1111/1541-4337.12059

Pickardt, C., Dongowski, G., & Kunzek, H. (2004). The influence of mechanical and enzymatic disintegration of carrots on the structure and properties of cell wall materials. *European Food Research and Technology*, *219*(3), 229–239. https://doi.org/10.1007/s00217-004-0960-z

Ramachandraiah, K., & Chin, K. B. (2016). Evaluation of ball-milling time on the physicochemical and antioxidant properties of persimmon by-products powder. *Innovative Food Science & Emerging Technologies*, *37*, 115–124. https://doi.org/10.1016/j.ifset.2016.08.005

Redgwell, R. J., Curti, D., & Gehin-Delval, C. (2008). Physicochemical properties of cell wall materials from apple, kiwifruit and tomato. *European Food Research and Technology*, *227*(2), 607–618. https://doi.org/10.1007/s00217-007-0762-1

Salehi, F. (2020). Physico-chemical and rheological properties of fruit and vegetable juices as affected by high pressure homogenization: A review. *International Journal of Food Properties*, *23*(1), 1136–1149. https://doi.org/10.1080/10942912.2020.1781167

Singh, S. S., Ghodki, B. M., & Goswami, T. K. (2018). Effect of grinding methods on powder quality of king chilli. *Journal of Food Measurement and Characterization*, *12*(3), 1686–1694. https://doi.org/10.1007/s11694-018-9784-6

Tan, J., & Kerr, W. L. (2015). Rheological properties and microstructure of tomato puree subject to continuous high pressure homogenization. *Journal of Food Engineering*, *166*, 45–54. https://doi.org/10.1016/j.jfoodeng.2015.05.025

Thebaudin, J. Y., Lefebvre, A. C., Harrington, M., & Bourgeois, C. M. (1997). Dietary fibres: Nutritional and technological interest. *Trends in Food Science & Technology*, *8*(2), 41–48. https://doi.org/10.1016/S0924-2244(97)01007-8

Van Audenhove, J., Bernaerts, T., De Smet, V., Delbaere, S., Van Loey, A. M., & Hendrickx, M. E. (2021). The Structure and Composition of Extracted Pectin and Residual Cell Wall Material from Processing Tomato: The Role of a Stepwise Approach versus High-Pressure Homogenization-Facilitated Acid Extraction. *Foods*, *10*(5), 1064. https://doi.org/10.3390/foods10051064

Van Audenhove, J., Bernaerts, T., Putri, N. I., Okello, E. O., Van Rooy, L., Van Loey, A. M., & Hendrickx, M. E. (2021). Microstructural and Texturizing Properties of Partially Pectin-Depleted Cell Wall Material: The Role of Botanical Origin and High-Pressure Homogenization. *Foods*, *10*(11), 2644. https://doi.org/10.3390/foods10112644

Van Buggenhout, S., Wallecan, J., Christiaens, S., Debon, S. J. J., Desmet, C., Van Loey, A., Hendrickx, M., & Mazoyer, J. (2015). Influence of high-pressure homogenization on functional properties of orange pulp. *Innovative Food Science and Emerging Technologies*, *30*, 51–60. https://doi.org/10.1016/j.ifset.2015.05.004

Vetter, S., & Kunzek, H. (2003). The influence of the sequential extractions on the structure and the properties of single cell materials from apples. *European Food Research and Technology*, *217*(5), 392–400. https://doi.org/10.1007/s00217-003-0767-3

Wang, J., Zhang, M., Devahastin, S., & Liu, Y. (2020). Influence of low-temperature ball milling time on physicochemical properties, flavor, bioactive compounds contents and antioxidant activity of horseradish powder. *Advanced Powder Technology*, *31*(3), 914–921. https://doi.org/10.1016/j.apt.2019.12.011

Wang, Y., Sun, P., Li, H., Adhikari, B. P., & Li, D. (2018). Rheological Behavior of Tomato Fiber Suspensions Produced by High Shear and High Pressure Homogenization and Their Application in Tomato Products. *International Journal of Analytical Chemistry*, Article ID 5081938. https://doi.org/10.1155/2018/5081938

Willemsen, K. L. D. D., Panozzo, A., Moelants, K., Cardinaels, R., Wallecan, J., Moldenaers, P., & Hendrickx, M. (2018). Effect of pH and salts on microstructure and viscoelastic properties of lemon peel acid insoluble fiber suspensions upon high pressure homogenization. *Food Hydrocolloids*, *82*, 144–154. https://doi.org/10.1016/j.foodhyd.2018.04.005

Willemsen, K. L. D. D., Panozzo, A., Moelants, K., Debon, S. J. J., Desmet, C., Cardinaels, R., Moldenaers, P., Wallecan, J., & Hendrickx, M. E. G. (2017). Physico-chemical and viscoelastic properties of high pressure homogenized lemon peel fiber fraction suspensions obtained after sequential pectin extraction. *Food Hydrocolloids*, *72*, 358–371. https://doi.org/10.1016/j.foodhyd.2017.06.020

Yeats, T., Vellosillo, T., Sorek, N., Ibáñez, A., & Bauer, S. (2016). Rapid Determination of Cellulose, Neutral Sugars, and Uronic Acids from Plant Cell Walls by One-step Two-step Hydrolysis and HPAEC-PAD. *Bio-Protocol*, *6*(20), e1978. https://doi.org/10.21769/bioprotoc.1978

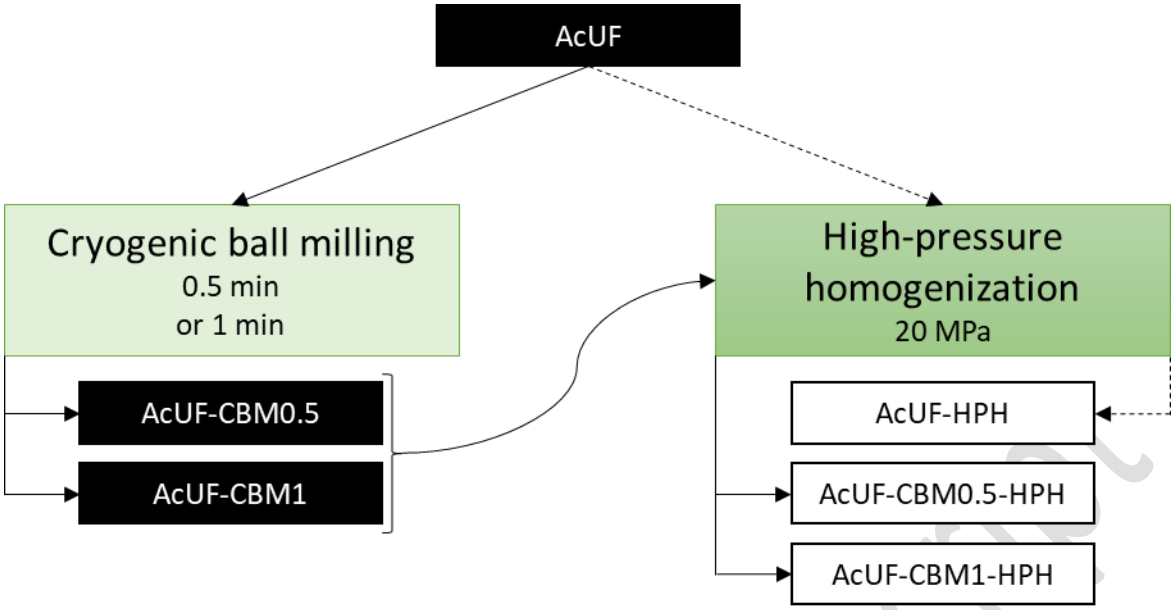

Figure 1: Overview of the particle size reduction techniques, i.e., cryogenic ball milling (CBM) and high-pressure homogenization (HPH) at 20 MPa, applied to the acid-unextractable fraction (AcUF) with indication of the naming of the treated AcUFs.

	no HPH	HPH
AcUF	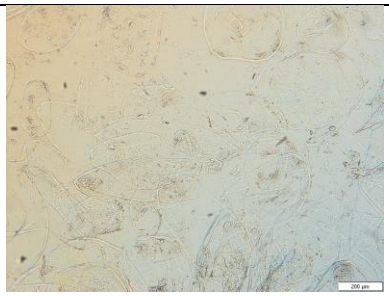	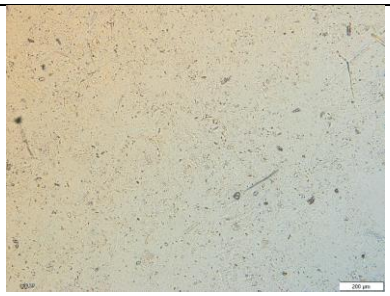
AcUF-CBM0.5	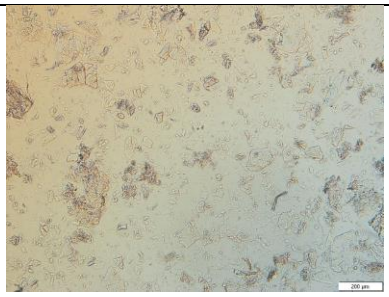	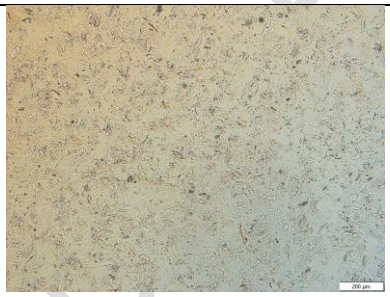
AcUF-CBM1	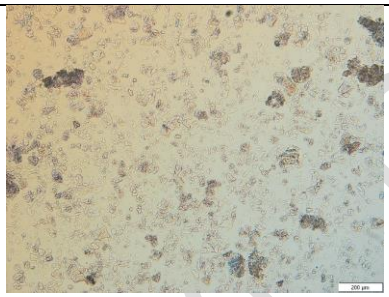	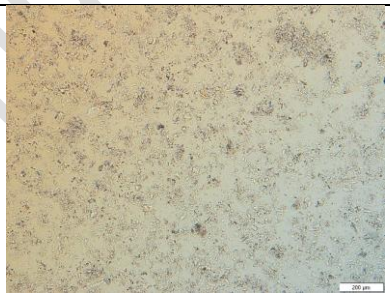

Figure 2: Micrographs of the suspensions (0.6% w/w) of the acid-unextractable fraction (AcUF) and cryogenic ball milled AcUF for 0.5 min (AcUF-CBM0.5) and 1 min (AcUF-CBM1) before and after high-pressure homogenization (HPH) at 20 MPa. The scale bar represents 200 µm.

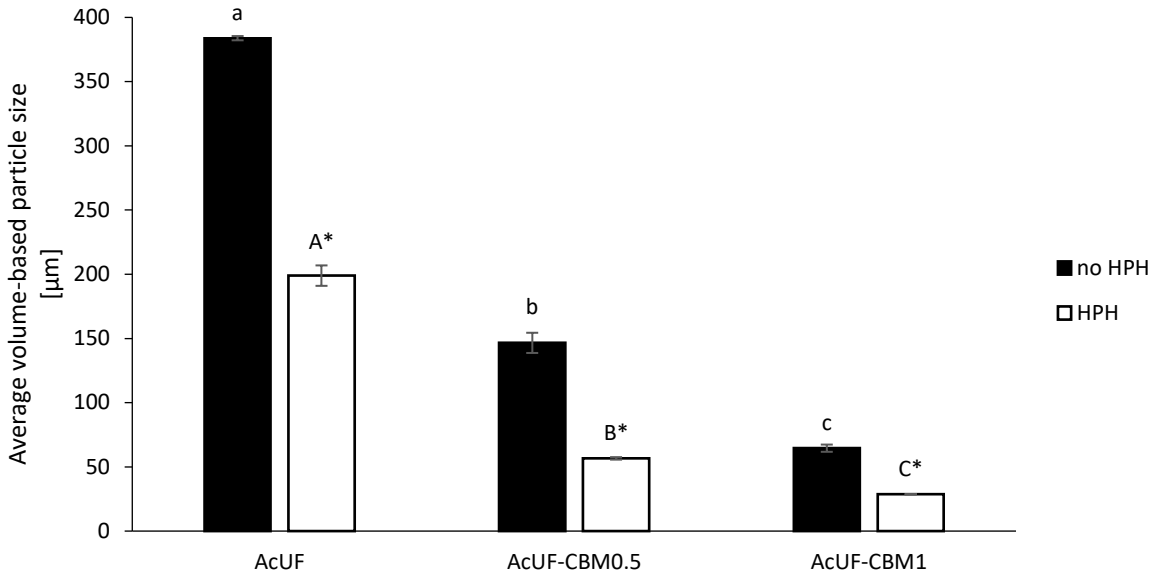

Figure 3: Average volume-based particle size ($d_{4,3}$) of the acid-unextractable fraction (AcUF) and cryogenic ball milled AcUF for 0.5 min (AcUF-CBM0.5) and 1 min (AcUF-CBM1) before and after high-pressure homogenization (HPH) at 20 MPa. The error bars correspond to the standard deviation. Different letters indicate significant differences for the suspensions before HPH (lower-case letters) and after HPH (higher-case letters) and an asterisk indicates a significant effect of HPH (Tukey test, $p < 0.05$).

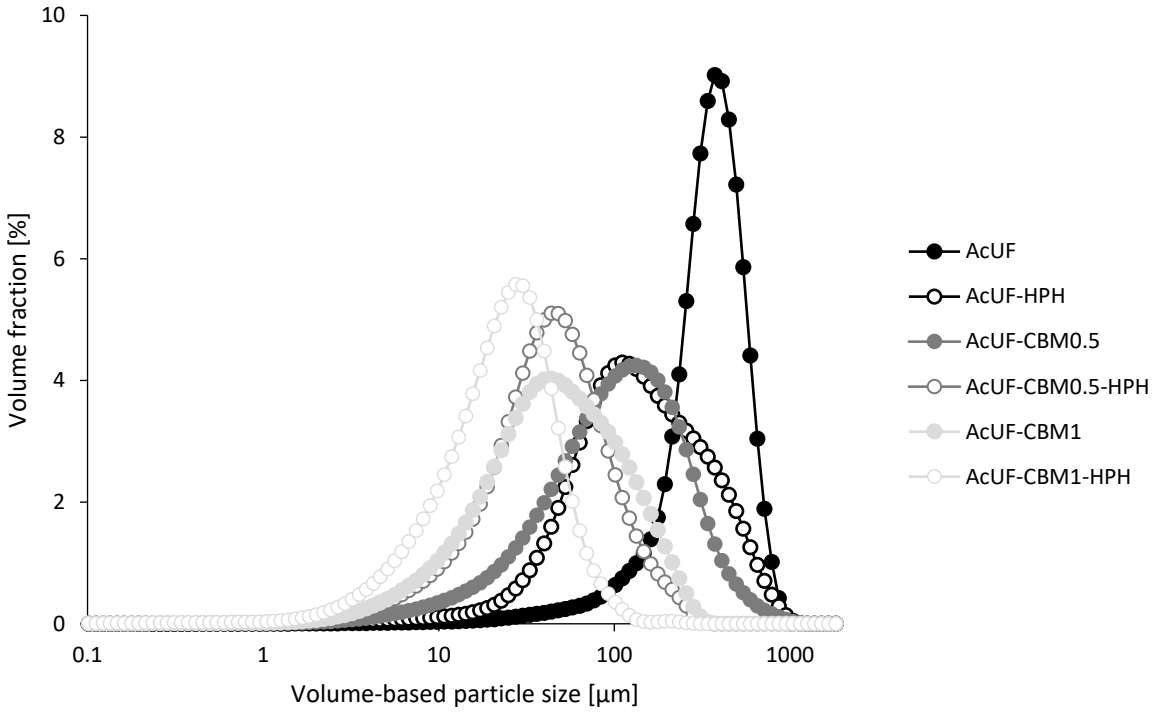

Figure 4: Volume-based particle size distribution of the suspensions of the acid-unextractable fraction (AcUF) and cryogenic ball milled AcUF for 0.5 min (AcUF-CBM0.5) and 1 min (AcUF-CBM1) before and after high-pressure homogenization (HPH) at 20 MPa.

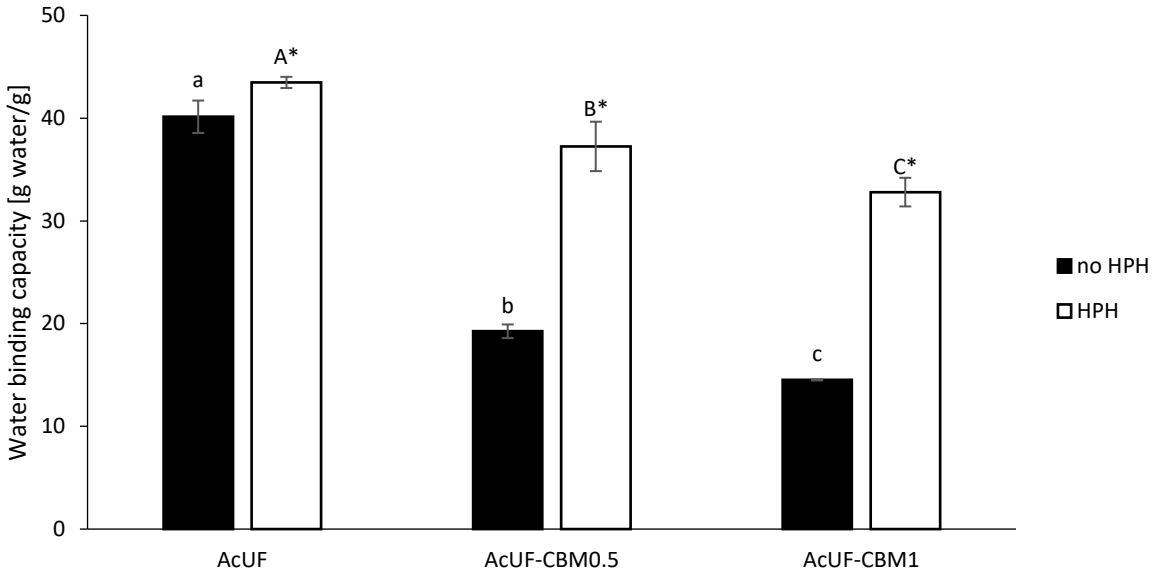

Figure 5: Water binding capacity (WBC) of the acid-unextractable fraction (AcUF) and cryogenic ball milled AcUF for 0.5 min (AcUF-CBM0.5) and 1 min (AcUF-CBM1) in suspension (2% w/w) before and after high-pressure homogenization (HPH) at 20 MPa. The error bars correspond to the standard deviation. Different letters indicate significant differences for the suspensions before HPH (lower-case letters) and after HPH (higher-case letters) and an asterisk indicates a significant effect of HPH (Tukey test, $p < 0.05$).

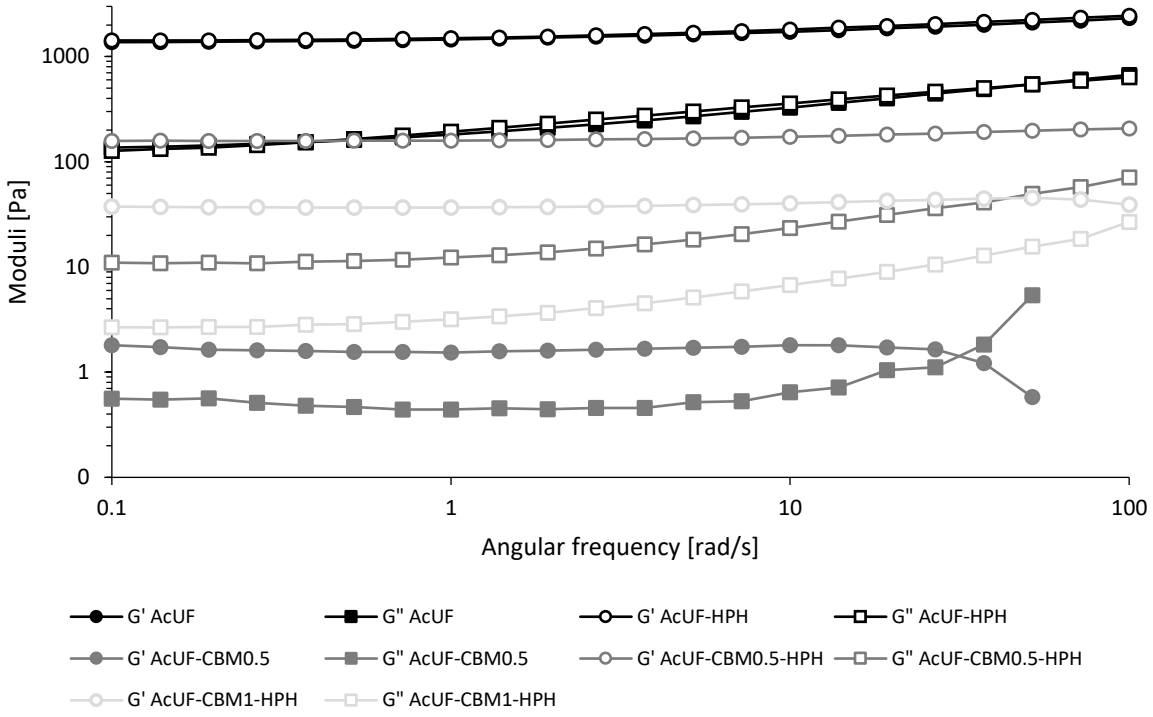

Figure 6: Storage modulus (G') and loss modulus (G") of the suspensions (2% w/w) of the acid-unextractable fraction (AcUF) and cryogenic ball milled AcUF for 0.5 min (AcUF-CBM0.5) and 1 min (AcUF-CBM1) before and after high-pressure homogenization (HPH) at 20 MPa as a function of the angular frequency (data are from the frequency sweep).

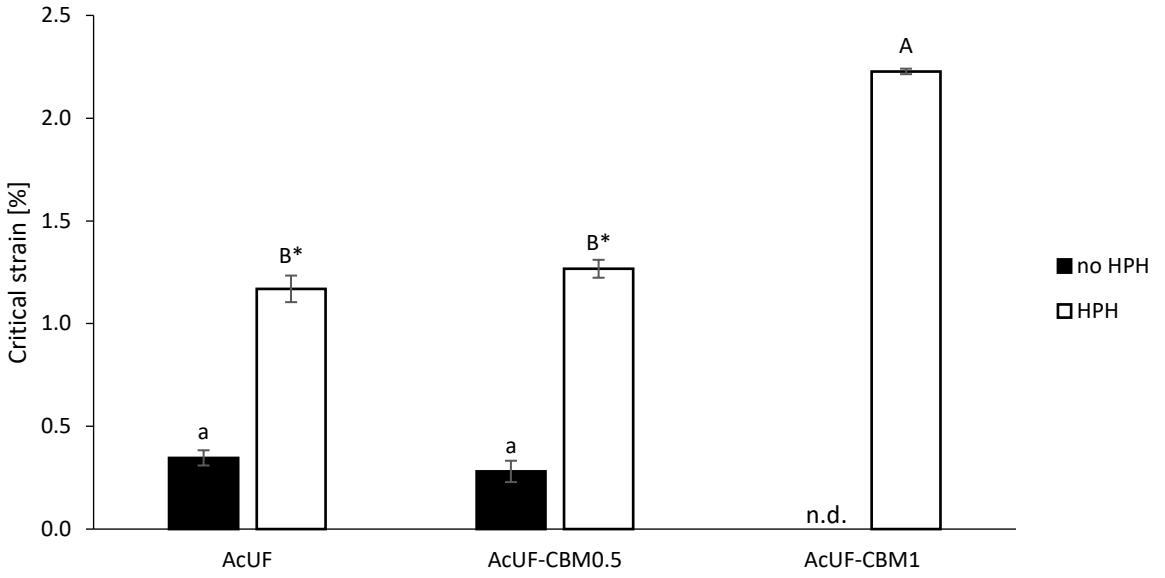

Figure 7: Critical strain at frequency 10 rad/s of the suspensions (2% w/w) of the acid-unextractable fraction (AcUF) and cryogenic ball milled AcUF for 0.5 min (AcUF-CBM0.5) and 1 min (AcUF-CBM1) before and after high-pressure homogenization (HPH) at 20 MPa (data are from the strain sweep). The error bars correspond to the standard deviation. Different letters indicate significant differences for the suspensions before HPH (lower-case letters) and after HPH (higher-case letters) and an asterisk indicates a significant effect of HPH (Tukey test, $p < 0.05$). n.d. = not determined, due to the instability of the AcUF-CBM1 suspension

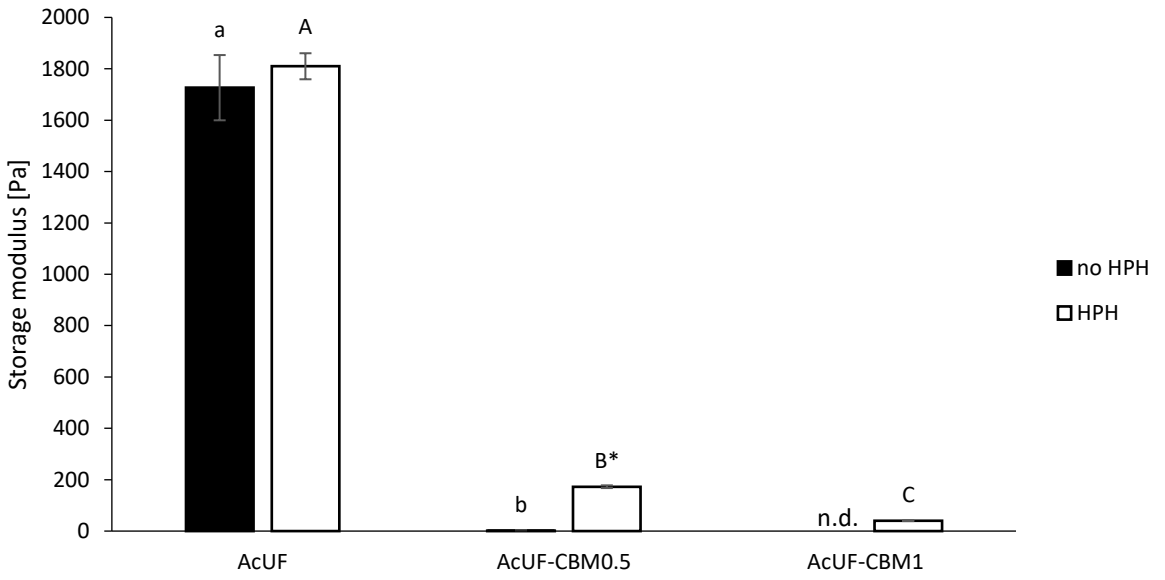

Figure 8: Storage modulus at frequency 10 rad/s and strain 0.1% of the suspensions (2% w/w) of the acid-unextractable fraction (AcUF) and cryogenic ball milled AcUF for 0.5 min (AcUF-CBM0.5) and 1 min (AcUF-CBM1) before and after high-pressure homogenization (HPH) at 20 MPa. The error bars correspond to the standard deviation. Different letters indicate significant differences for the suspensions before HPH (lower-case letters) and after HPH (higher-case letters) and an asterisk indicates a significant effect of HPH (Tukey test, $p < 0.05$). n.d. = not determined, due to the instability of the AcUF-CBM1 suspension

Table 1: Monosaccharide content and degree of methyl esterification (DM) of the acid-unextractable fraction (AcUF) ± standard deviation.

	Monosaccharide content [mg/g]							
	Rha	Ara	Gal	Glc	Xyl	Man	UA	DM [%]
AcUF	5.2 ± 0.6	7.8 ± 0.2	12.8 ± 1.3	412.5 ± 23.7	51.4 ± 4.6	39.4 ± 1.4	186.9 ± 4.6	55.6 ± 2.8